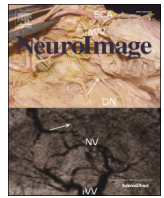




Contents lists available at ScienceDirect

NeuroImage

journal homepage: www.elsevier.com/locate/ynimg

Validation of quantitative susceptibility mapping with Perls' iron staining for subcortical gray matter

Hongfu Sun^a, Andrew J. Walsh^a, R. Marc Lebel^a, Gregg Blevins^b, Ingrid Catz^b, Jian-Qiang Lu^c, Edward S. Johnson^c, Derek J. Emery^d, Kenneth G. Warren^b, Alan H. Wilman^{a,*}

^a Department of Biomedical Engineering, University of Alberta, Edmonton, Alberta, Canada, T6G 2V2

^b Division of Neurology, Department of Medicine, University of Alberta, Edmonton, Alberta, Canada, T6G 2G3

^c Department of Laboratory Medicine and Pathology, University of Alberta, Edmonton, Alberta, Canada, T6G 2B7

^d Department of Radiology and Diagnostic Imaging, University of Alberta, Edmonton, Alberta, Canada, T6G 2B7

ARTICLE INFO

Article history:

Accepted 4 November 2014

Available online xxxxx

Keywords:

Quantitative susceptibility mapping

Postmortem imaging

Perls' iron stain

Brain iron

Subcortical gray matter

R2* mapping

ABSTRACT

Quantitative susceptibility mapping (QSM) measures bulk susceptibilities in the brain, which can arise from many sources. In iron-rich subcortical gray matter (GM), non-heme iron is a dominant susceptibility source. We evaluated the use of QSM for iron mapping in subcortical GM by direct comparison to tissue iron staining. We performed *in situ* or *in vivo* QSM at 4.7 T combined with Perls' ferric iron staining on the corresponding extracted subcortical GM regions. This histochemical process enabled examination of ferric iron in complete slices that could be related to susceptibility measurements. Correlation analyses were performed on an individual-by-individual basis and high linear correlations between susceptibility and Perls' iron stain were found for the three multiple sclerosis (MS) subjects studied ($R^2 = 0.75, 0.62, 0.86$). In addition, high linear correlations between susceptibility and transverse relaxation rate ($R2^*$) were found ($R^2 = 0.88, 0.88, 0.87$) which matched *in vivo* healthy subjects ($R^2 = 0.87$). This work validates the accuracy of QSM for brain iron mapping and also confirms ferric iron as the dominant susceptibility source in subcortical GM, by demonstrating high linear correlation of QSM to Perls' ferric iron staining.

© 2014 Elsevier Inc. All rights reserved.

Introduction

Iron accumulation in subcortical gray matter (GM) may serve as an important biomarker of normal aging (Aquino et al., 2009; Cherubini et al., 2009; Hallgren and Sourander, 1958; Schenck and Zimmerman, 2004), and of neurological diseases including Alzheimer's disease, Parkinson's disease, Huntington's disease and multiple sclerosis (MS) (Berg and Youdim, 2006; Chen et al., 1993; Dexter et al., 1991; Khalil et al., 2011; LeVine, 1997; Williams et al., 2012). The mechanisms behind iron accumulation are not yet fully understood, although iron may accumulate through inflammatory and destructive processes (Stephenson et al., 2014), and may relate to the presence and extent of neurodegeneration. Measuring the state of brain iron metabolism may provide important information on aging and neurological diseases.

Abbreviations: QSM, quantitative susceptibility mapping; EDSS, Expanded Disability Status Scale; PRELUDE, Phase Region Expanding Labeller for Unwrapping Discrete Estimates; SHARP, Sophisticated Harmonic Artifact Reduction for Phase data; RESHARP, Regularization Enabled SHARP; TV, total variation; GP, globus pallidus; PU, putamen; CN, caudate nucleus; RN, red nucleus; SN, substantia nigra; TH, thalamus.

* Corresponding author at: Department of Biomedical Engineering, University of Alberta, 1098 Research Transition Facility, Edmonton, Alberta, T6G 2V2, Canada.

E-mail address: wilman@ualberta.ca (A.H. Wilman).

MRI provides a variety of contrast mechanisms that are sensitive to brain iron (Haacke et al., 2005) including transverse relaxation rates $R2$ and $R2^*$, and susceptibility methods such as phase and susceptibility-weighted imaging. Previous studies in healthy subjects have shown that $R2$ and $R2^*$ increase in iron-rich brain regions and correlate strongly with iron concentration (Drayer et al., 1986; Gelman et al., 1999; Langkammer et al., 2010; Li et al., 2009; Peran et al., 2007; Thomas et al., 1993). While sensitive to iron, $R2$ and $R2^*$ may be affected by other sources such as macromolecular and water content changes (Mitsumori et al., 2012), which makes them not specific to brain iron. The introduction of phase imaging minimizes the influence of changes in macromolecular and water content, and is able to distinguish between negative and positive susceptibility sources (Duyn et al., 2007; Haacke et al., 2004; Rauscher et al., 2005). In addition, phase imaging has demonstrated good correlation to brain iron in subcortical GM (Haacke et al., 2007; Ogg et al., 1999; Yao et al., 2009). However, the non-local field properties of phase imaging cause it to be dependent on the shape and orientation of the object to the main magnetic field (Li and Leigh, 2004; Marques et al., 2009), which complicates interpretation.

The developing field of quantitative susceptibility mapping (QSM) inherits the iron sensitivity from phase imaging while eliminating the problem of non-locality. Derived from a deconvolution process from

<http://dx.doi.org/10.1016/j.neuroimage.2014.11.010>

1053-8119/© 2014 Elsevier Inc. All rights reserved.

Please cite this article as: Sun, H., et al., Validation of quantitative susceptibility mapping with Perls' iron staining for subcortical gray matter, NeuroImage (2014), <http://dx.doi.org/10.1016/j.neuroimage.2014.11.010>

phase images, QSM unveils the local tissue susceptibility directly (de Rochefort et al., 2010; Kressler et al., 2010; Li et al., 2011; Liu et al., 2009, 2011; Reichenbach, 2012; Schweser et al., 2011; Shmueli et al., 2009; Wharton and Bowtell, 2010). A number of in vivo susceptibility maps have shown good correlations with subcortical GM iron concentrations (Bilgic et al., 2012; Schweser et al., 2011; Wu et al., 2012) as estimated from the hallmark study on brain iron by Hallgren and Sourander (1958). Nevertheless, validation of QSM for brain iron mapping requires postmortem studies that make a direct comparison between MRI and histochemistry. Only two human postmortem studies have been performed to date that compare QSM to histochemically measured iron content in subcortical GM. These studies used mass spectrometry (Langkammer et al., 2012) or X-ray emission and fluorescence (Zheng et al., 2013). The Langkammer et al. (2012) study provided absolute iron values but in small samples that do not provide a full spatial map of the tissue to relate to the susceptibility map, while the work by Zheng et al. (2013) used previously frozen formalin fixed tissue for MRI rather than in situ imaging. Furthermore, both studies examined total iron (ferrous and ferric). Thus to further validate QSM for subcortical GM iron mapping and to verify ferric iron as the main susceptibility source, there remains a need to compare in situ and in vivo susceptibility maps directly to spatial maps of ferric iron. In this study, we make use of Perls' iron staining (Meguro et al., 2007) to obtain full slice spatial maps of relative ferric iron content and compare to in situ and in vivo QSM in subcortical GM.

Material and methods

Subjects

In situ or in vivo QSM followed by Perls' iron staining was performed on three subjects who have been previously studied for phase, R_2^* , and R_2^* mapping (Walsh et al., 2013). Subject 1 was a 63 year old male imaged in situ 28 h after death. Subject 2 was a 60 year old male imaged in situ 7 h after death. Subject 3 was a 45 year old male imaged in vivo one year before death. Subjects 1 and 2 had secondary progressive MS with Expanded Disability Status Scale (EDSS) scores of 8.5 before death, and disease durations of approximately 40 years. Subject 3 had relapsing remitting MS for 7 years with EDSS of 3.5 at time of imaging. Postmortem brains were fixed in formalin for 2 weeks, 6 months, and 6 weeks respectively before extraction for Perls' iron staining. The brain temperatures of postmortem Subject 1 and 2 were $\sim 29^\circ\text{C}$ and 14°C during MRI as estimated according to Al-Alousi et al. (2001). In addition, QSM and R_2^* were performed on three healthy male volunteers (age 48 ± 6 yrs). For all subjects, institutional ethical approval and informed consent from the subjects and/or their families were obtained.

MRI acquisition

Three-dimensional multiple gradient-echo acquisitions were collected at 4.7 T (Varian, Palo Alto, CA) either in situ or in vivo. Acquisition parameters were: field-of-view $256 \times 128 \times 160$ mm; spatial resolution $1 \times 0.8 \times 2$ mm; 80 axial slices; TR 44 ms; 10 echoes with echo spacing 4.1 ms; first echo time 2.9–3.2 ms; flip angle 10° ; readout bandwidth 352 Hz/voxel; total acquisition time 8.9 min. A birdcage head coil was used for radiofrequency transmission and a tight-fitting 4-channel array coil for signal reception. The raw k-space datasets were saved and moved offline for image reconstruction.

Image reconstruction

Susceptibility maps were reconstructed from the raw phase images, following three main steps: phase pre-processing, background field artifact removal, and susceptibility inversion, as demonstrated in Fig. 1. In the phase pre-processing step, raw phase measures from the 4

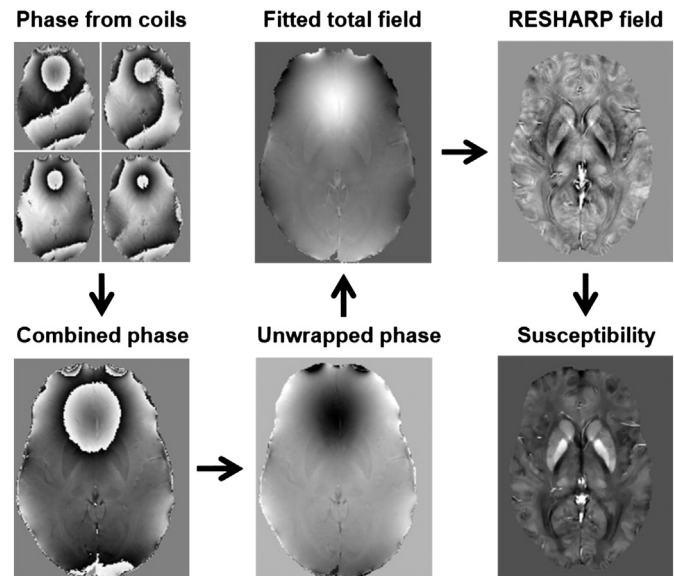


Fig. 1. The workflow for generating susceptibility maps from raw phase measurements. Phase-arrayed coils were combined after removing phase-offsets, and unwrapped using PRELUDE, then fitted to echo times. Background field was then removed using RESHARP, followed by susceptibility inversion using total variation regularization.

independent receiver channels were combined after removing the receiver phase offsets estimated from the first two echoes as previously described (Robinson et al., 2011). The brain was extracted using the brain extraction tool (Smith, 2002) of FMRIB software library (FSL) on each echo. Aliased phase images were unwrapped in 3D with Phase Region Expanding Labeller for Unwrapping Discrete Estimates (PRELUDE) (Jenkinson, 2003) of FSL. A single field map was generated by linearly fitting the unwrapped phase maps to echo times, weighted by the masked magnitudes of each echo to increase the reliability of the fitting. Background field, mainly due to air-tissue susceptibility interfaces, was removed using RESHARP (“Regularization Enabled Sophisticated Harmonic Artifact Reduction for Phase data”) (Sun and Wilman, 2013), which applies Tikhonov regularization on SHARP (“Sophisticated Harmonic Artifact Reduction for Phase data”) (Schweser et al., 2011) to suppress non-harmonic artifacts from sources other than air-tissue susceptibility interfaces. The Tikhonov regularization parameter was set to 1×10^{-3} determined by the L-curve method. Finally, single-angle dipole inversion from local field to susceptibility was performed using the total variation (TV) regularization approach, which is the L1 norm of the gradients, and is similar to Bilgic et al. (2012), Liu et al. (2011), and Wu et al. (2012), with regularization parameter on the TV term selected as 5×10^{-4} by the L-curve method, after normalization to the main magnetic field in the unit of parts-per-million (ppm). In addition to susceptibility maps, R_2^* maps were also reconstructed as previously described (Lebel et al., 2012), using mono-exponential fit of all echoes, after a linear field gradient correction to compensate the air-tissue susceptibility dephasing effect.

Perls' iron staining and photographic processing

The brains of the subjects were removed at postmortem in accord with standard autopsy protocol, fixed in 18% formalin, and sectioned in 8 mm slices. Subject 1 was cut axially, while Subject 2 and 3 were cut in standard coronal sections. Slices containing subcortical GM were photographed and then stained with Perls' iron reagents (Meguro et al., 2007) by immersing in 1 L of 2% hydrochloric acid mixed with

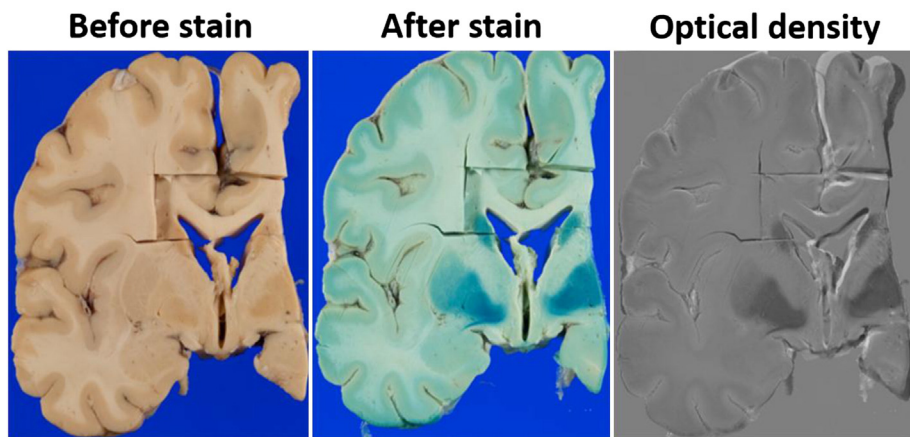


Fig. 2. Production of an optical density map of a coronal slice from Subject 1. Slice was photographed before and after Perls' iron staining. Registered photographs were normalized to gray scales then subtracted to produce the optical density map.

1 L of 2% potassium ferrocyanide for 30 min. The stained slices were then photographed again after washing off the residual staining solution with running water. Processing steps for combining unstained and stained photographs are demonstrated in Fig. 2. For each slice set of photographs, conversion to gray scale was made with the window and level of the stained photographs adjusted to match that of the unstained photographs by using two reference points: the background blue photographic paper and a region of unstained white matter. The intensity differences of the stained and unstained photographs were then normalized after division by the intensity difference between the background and the unstained white matter reference region for each slice. An image of relative optical density was produced, where a higher value corresponds to greater iron staining. This method has been previously applied for quantitative iron validation by our group and others (Bizzi et al., 1990; Walsh et al., 2013).

Regions of interest selection

Regions of interest (ROIs) in iron rich basal ganglia and thalamus were drawn encompassing the full structure on each available Perls' iron staining slice including: globus pallidus (GP), putamen (PU), caudate nucleus (CN), red nucleus (RN), substantia nigra (SN) and thalamus (TH). These ROIs were transferred onto the registered unstained maps. ROIs were drawn on stained photographs which supply higher contrast boundaries than unstained ones. This boundary could be bias if areas of structure did not stain. However, it is our experience, including past work (Walsh et al., 2013), that the territorial boundaries on stained or unstained photographs are similar. Susceptibility and $R2^*$ maps were manually rigid registered to pathological photographs, and MRI ROIs were drawn on susceptibility maps according to borders of regions. The same ROIs from susceptibility maps were also transferred onto the

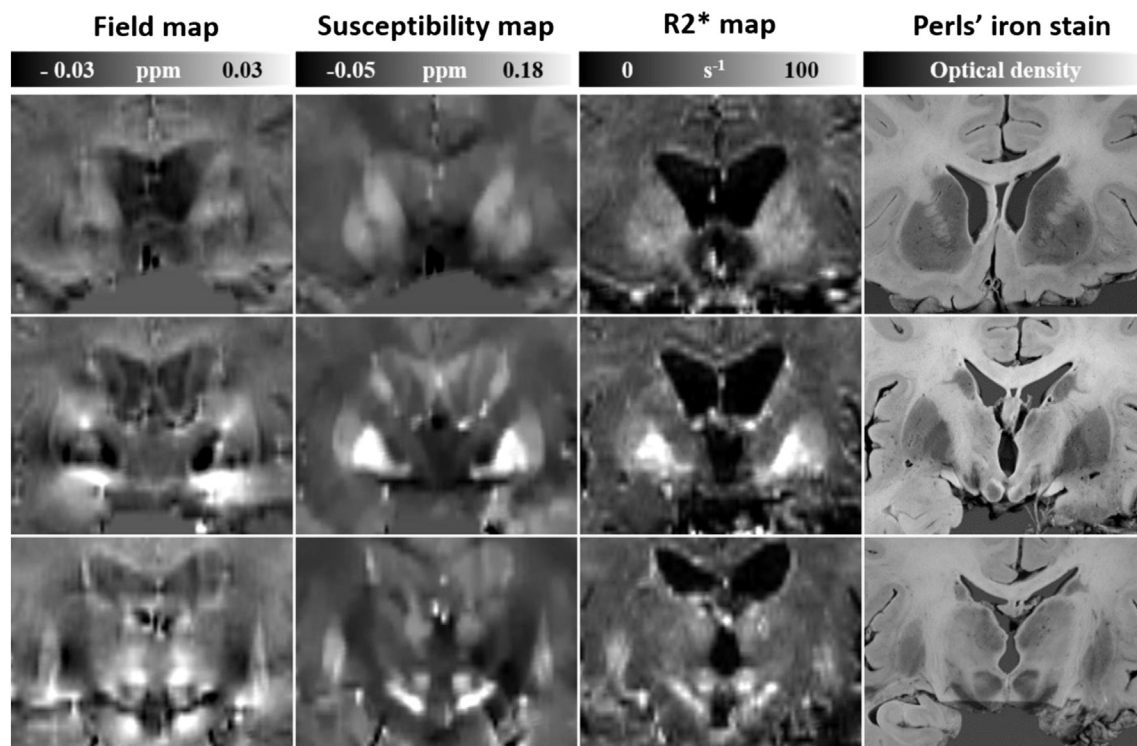


Fig. 3. Local field, susceptibility, and $R2^*$ maps and corresponding Perls' iron stains of three coronal slices (in rows) from Subject 3 (45-years-male) scanned in vivo 1 year before death.

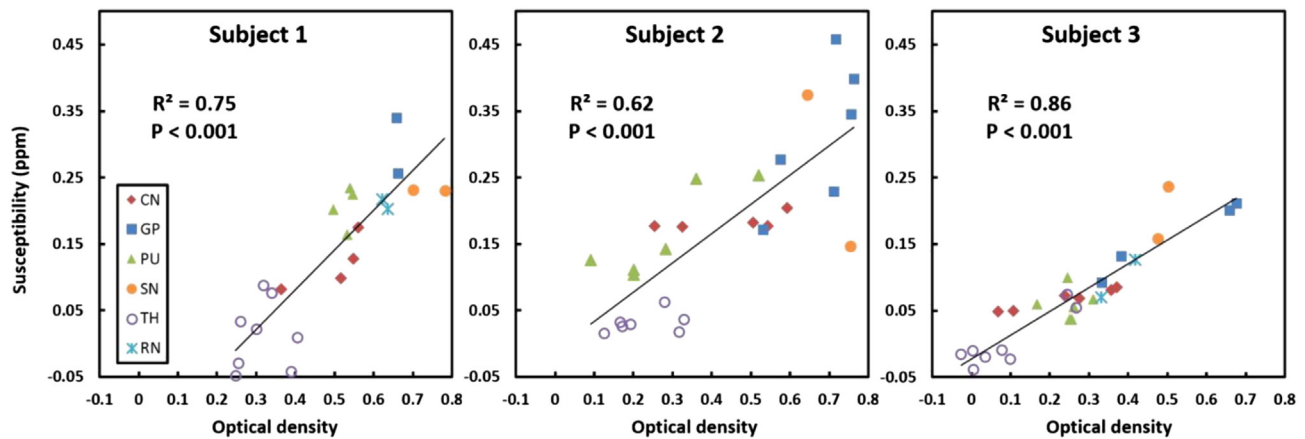


Fig. 4. Correlations of susceptibility with Perls' iron stain (optical density) for the three subjects. Red nucleus is absent in Subject 2 due to unavailability of this pathological cut.

corresponding R^2 maps. Each structure was measured on both left and right sides and on multiple slices when available, and mean values were recorded for whole ROIs.

Correlation analysis

The Pearson correlation coefficient was calculated for mean susceptibility to Perls' iron staining optical density of the subcortical GM regions for each postmortem subject. Susceptibility to R^2 correlation was also performed in the postmortem subjects and in vivo healthy subjects. All correlations were calculated with linear least-squares regressions using SPSS software (IBM, Armonk, NY). Susceptibility measurements were relative to that of cerebrospinal fluid (CSF) at the anterior portion of the lateral ventricles.

Results

Fig. 3 illustrates three coronal brain images from Subject 3 (in vivo) including field, susceptibility, and R^2 maps and the Perls' iron stains. The field maps suffer from strong dipole effects which are resolved in the susceptibility maps, providing clear delineation between iron-rich regions. Subcortical GM hyperintensities in susceptibility and R^2 maps correspond well to hypointensities in Perls' iron stains.

The resulting correlations of susceptibility to Perls' iron stain are shown in Fig. 4. Perls' iron stain is in the form of optical density with higher value meaning greater iron density. Strong linear correlations were found for all subjects, with coefficients of $R^2 = 0.75, 0.62,$ and 0.86 respectively. All the correlations are significant with $P < 0.001$. Correlations were analyzed individually on each subject due to different disease stages and different fixation time in formalin between MRI and histochemistry. Mean susceptibility values of subcortical GM regions in two in situ postmortem cases were larger than those found in vivo. For example, the mean susceptibility of GP was 0.31 ppm from the two in situ subjects as compared to 0.20 ppm from the in vivo Subject 3. This may be due to the fully deoxygenated blood with high susceptibility values in situ, which may be a confound of in situ imaging, leading to a higher correlation in the in vivo Subject 3, although the ages and disease stages were also different.

Susceptibility results were also correlated to R^2 from the same regions using the three MS subjects and additional three healthy in vivo subjects. Example axial images of susceptibility and R^2 from one healthy in vivo subject are shown in Fig. 5, where the susceptibility maps more clearly delineate the subcortical GM territories and appear smoother than R^2 . Statistical analysis found high linear correlations between susceptibility and R^2 for all three MS subjects ($R^2 = 0.88, 0.88, 0.87$), and a similarly high correlation was also obtained from the

three in vivo healthy subjects with $R^2 = 0.87$ as shown in Fig. 6. All the correlations are significant with $P < 0.001$. The slopes and intercepts are very similar among in vivo healthy subjects and in vivo Subject 3 (bottom row), while greater variation is seen between the two in situ subjects (top row).

Discussion

To compare susceptibility directly to ferric iron, we performed whole slice Perls' iron staining after in vivo or in situ QSM. This process enabled similar large ROI analysis on both MRI and Perls' stains, rather than highly localized samples. Furthermore, we performed in situ MRI shortly after death, to avoid extraction and fixation which can substantially alter MRI properties (Dawe et al., 2009; van Duijn et al., 2011). Our approach yielded high correlations between susceptibility and ferric iron ($R^2 = 0.75, 0.62, 0.86$), including measures of GP, PU, CN, thalamus, RN and SN. Highest correlation was found in the in vivo subject, without confound of fully deoxygenated blood. Our correlations using only in

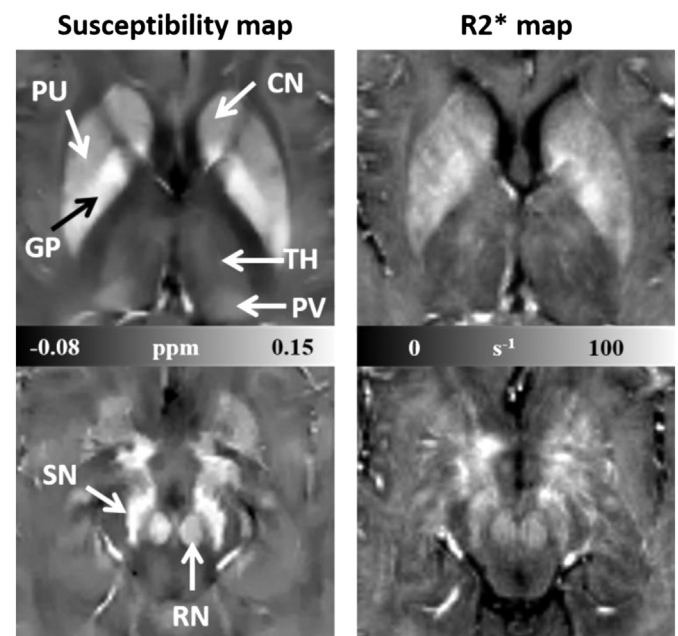


Fig. 5. Axial susceptibility (left) and R^2 (right) maps of a healthy subject (48 yrs-old male). Subcortical GM structures are demonstrated with arrows: CN (caudate nucleus), PU (putamen), GP (globus pallidus), TH (thalamus), PV (pulvinar), SN (substantia nigra), and RN (red nucleus).

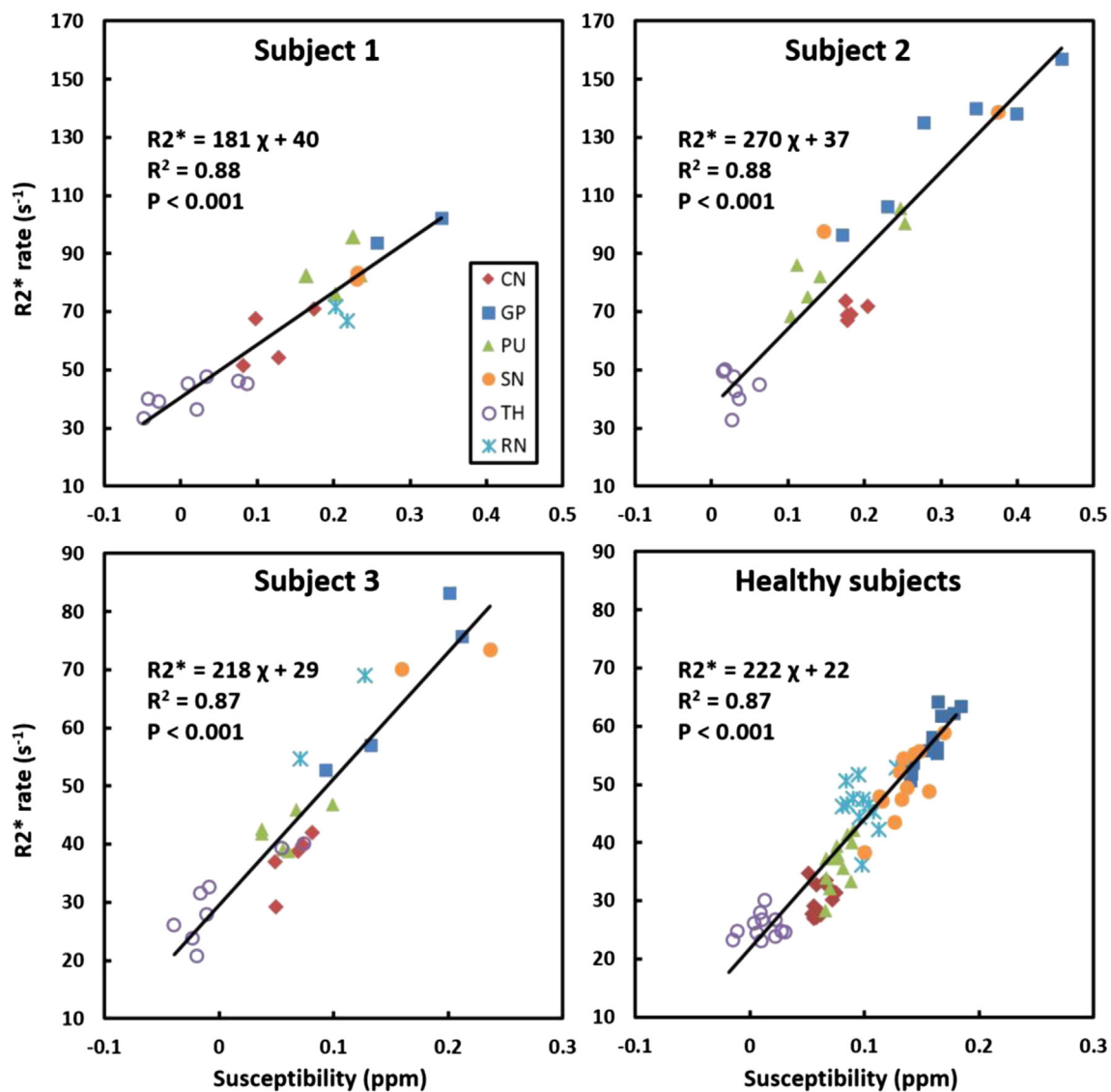


Fig. 6. Correlations of susceptibility with $R2^*$ for the three MS subjects and three healthy subjects. Note that the axes for in situ subjects (top row) and in vivo subjects (bottom row) have different scales.

situ subjects were similar to those of Langkammer et al. (2012) where in situ susceptibility correlations with iron of $R^2 = 0.71$ were found using GP, PU, CN and thalamus from 13 subjects with no history of neurological disorder. Our in situ results were also similar to the ex vivo work of Zheng et al. (2013) using one slice of previously frozen MS brain tissue ($R^2 = 0.55$ and 0.76), including only caudate, GP and PU. Previous studies measured total iron, while the Perls' method stained for only ferric iron which is the form of iron stored in ferritin (Drayer et al., 1986). Our work verifies that ferric iron alone provides a high correlation to susceptibility and is the main source of subcortical GM susceptibility contrast.

As well as susceptibility, $R2^*$ has been used in previous postmortem studies for subcortical GM iron measurements. Similar correlations were found in our previous $R2^*$ validation study (Walsh et al., 2013) with $R^2 = 0.69, 0.63,$ and 0.86 for the same subjects using Perls' iron staining. Also Langkammer et al. (2010) reported $R2^*$ correlation to plasma mass spectrometry iron with $R^2 = 0.87$ using small localized samples. Both susceptibility and $R2^*$ are clearly useful and sensitive markers for brain iron mapping, provided iron is the dominant image contrast. Our results (Fig. 6) confirmed high correlations between susceptibility and $R2^*$, with similarly high linear correlations for all subjects, in situ or in vivo.

When comparing QSM and $R2^*$ for brain iron mapping, each has its own advantages. QSM is the direct quantitative measure of susceptibility, which can be influenced by iron, but also myelin and calcium and other susceptibility sources, while $R2^*$ is the measure of signal decay within a voxel influenced by susceptibility induced field perturbation ($R2'$ dephasing effect) but also by macromolecule and water content ($R2$ diffusion effect). Therefore $R2^*$ and QSM for brain iron mapping can be influenced differently by factors such as water and myelin content. For the MS subjects studied here, demyelination, inflammation, atrophy and iron accumulation may vary between subjects and between structures, leading to variation in the slope and intercept in Fig. 6. A recent large in vivo study (Li et al., 2014) of healthy volunteers at 3 T published a $R2^*$ vs susceptibility plot with reduced slope to our in vivo subjects, likely due to use of a lower field strength since $R2^*$ is magnetic field strength dependent, while susceptibility contrast appears unchanged with field strength. At higher field strengths, increased susceptibility induced field dephasing increases sensitivity of $R2^*$ to ferric iron (Schenck and Zimmerman, 2004; Zhang et al., 2007). Moreover, $R2^*$ fitting is voxel-based, preserving spatial variation, while susceptibility inversion requires regularization to suppress noise amplification which blurs images somewhat within borders (Wharton and Bowtell,

2010), but provides better boundary delineation than $R2^*$ as can be seen from Fig. 5. With the current trend towards multiple gradient echo sequences for QSM, both $R2^*$ and QSM can be reconstructed from the same acquisition, providing complementary iron measures.

Limitations of this work include the fact that *in situ* MRI has fully deoxygenated blood presenting strong susceptibility sources from all vasculature; however blood is not present in Perls' iron stains. Our results suggest that fully deoxygenated blood vessels may increase the susceptibility values of subcortical GM measurements and degrade the correlation with Perls' iron stain (Fig. 4). Nevertheless, *in situ* correlations remained high. In addition, pathology cuts are of 8 mm thickness which may lead to variable locations between subjects for iron correlation to MRI. Another limitation is Perls' iron staining did not enable quantification of actual iron concentration, but only provided a relative measure. However, macroscopic maps of the tissue were possible with this approach, enabling two-dimensional large ROI selection in the same manner as standard *in vivo* MRI. In this study, we used MS subjects for postmortem validation, where different disease processes could be confounding factors. For example, Subject 2 has greater values of $R2^*$ and susceptibility in some of the GP and SN regions, indicating more iron accumulation, which is likely disease related. However, high linear correlations were still found for all MS subjects and $R2^*$ vs QSM slope and intercept of Subject 3 matched that of healthy *in vivo* subjects (Fig. 6). A further limitation is that the temperature of postmortem MRI scans were different than *in vivo* due to various cooling time. As previously reported, $R2'$ of basal ganglia increases with lower temperature (Birkl et al., 2014), and therefore $R2'$ of Subject 1 and 2 would increase as compared to *in vivo* scans due to the temperature differences. Another report (Langkammer et al., 2012) stated that paramagnetic susceptibility is approximately inversely proportional to temperature. Therefore susceptibilities at 14 °C and 29 °C increase 8% and 2% as compared to *in vivo* body temperature. The temperature effect on our measurements is thus expected to be small. Moreover, our correlations are analyzed individually to limit these effects.

In conclusion, subcortical GM susceptibilities measured from both *in situ* and *in vivo* MRI using MS subjects had strong linear correlations to ferric iron as determined by whole slice Perls' iron staining. These findings suggest that ferric iron is the dominant susceptibility source in subcortical GM in MS and that QSM can serve as a reliable ferric iron mapping method in iron-rich GM regions such as thalamus and basal ganglia.

Acknowledgments

Grant support from Canadian Institute of Health Research (MOP102582) and the Multiple Sclerosis Society of Canada (EGID1619) is acknowledged.

References

- Al-Alousi, L.M., Anderson, R.A., Worster, D.M., Land, D.V., 2001. Multiple-probe thermography for estimating the postmortem interval: II. Practical versions of the Triple-Exponential Formulae (TEF) for estimating the time of death in the field. *J. Forensic Sci.* 46, 323–327.
- Aquino, D., Bizzi, A., Grisoli, M., Garavaglia, B., Bruzzone, M.G., Nardocci, N., Savoiardo, M., Chiapparini, L., 2009. Age-related iron deposition in the basal ganglia: quantitative analysis in healthy subjects. *Radiology* 252, 165–172. <http://dx.doi.org/10.1148/radiol.2522081399>.
- Berg, D., Youdim, M.B.H., 2006. Role of iron in neurodegenerative disorders. *Top. Magn. Reson. Imaging* 17, 5–17. <http://dx.doi.org/10.1097/01.mrm.0000245461.90406.ad>.
- Bilgic, B., Pfefferbaum, A., Rohlfing, T., Sullivan, E.V., Adalsteinsson, E., 2012. MRI estimates of brain iron concentration in normal aging using quantitative susceptibility mapping. *Neuroimage* 59, 2625–2635. <http://dx.doi.org/10.1016/j.neuroimage.2011.08.077>.
- Birkl, C., Langkammer, C., Krenn, H., Goessler, W., Ernst, C., Haybaeck, J., Stollberger, R., Fazekas, F., Ropele, S., 2014. Iron mapping using the temperature dependency of the magnetic susceptibility. *Magn. Reson. Med.* 00, 1–7. <http://dx.doi.org/10.1002/mrm.25236>.
- Bizzi, A., Brooks, R.A., Brunetti, A., Hill, J.M., Alger, J.R., Miletich, R.S., Francavilla, T.L., Di Chiro, G., 1990. Role of iron and ferritin in MR imaging of the brain: a study in primates at different field strengths. *Radiology* 177, 59–65.
- Chen, J.C., Hardy, P.A., Kucharczyk, W., Clauberg, M., Joshi, J.G., Vourlas, A., Dhar, M., Henkelman, R.M., 1993. MR of human postmortem brain tissue: correlative study between T2 and assays of iron and ferritin in Parkinson and Huntington disease. *AJNR Am. J. Neuroradiol.* 14, 275–281.
- Cherubini, A., Péran, P., Caltagirone, C., Sabatini, U., Spalletta, G., 2009. Aging of subcortical nuclei: microstructural, mineralization and atrophy modifications measured *in vivo* using MRI. *Neuroimage* 48, 29–36. <http://dx.doi.org/10.1016/j.neuroimage.2009.06.035>.
- Dawe, R.J., Bennett, D.A., Schneider, J.A., Vasireddi, S.K., Arfanakis, K., 2009. Postmortem MRI of human brain hemispheres: T2 relaxation times during formaldehyde fixation. *Magn. Reson. Med.* 61, 810–818. <http://dx.doi.org/10.1002/mrm.21909>.
- De Rochefort, L., Liu, T., Kressler, B., Liu, J., Spincemaille, P., Lebon, V., Wu, J., Wang, Y., 2010. Quantitative susceptibility map reconstruction from MR phase data using bayesian regularization: validation and application to brain imaging. *Magn. Reson. Med.* 63, 194–206. <http://dx.doi.org/10.1002/mrm.22187>.
- Dexter, D.T., Carayon, A., Javoy-Agid, F., Agid, Y., Wells, F.R., Daniel, S.E., Lees, A.J., Jenner, P., Marsden, C.D., 1991. Alterations in the levels of iron, ferritin and other trace metals in Parkinson's disease and other neurodegenerative diseases affecting the basal ganglia. *Brain* 114 (Pt 4), 1953–1975. <http://dx.doi.org/10.1093/brain/114.4.1953>.
- Drayer, B., Burger, P., Darwin, R., Riederer, S., Herfkens, R., Johnson, G.A., 1986. MRI of brain iron. *AJ. Am. J. Roentgenol.* <http://dx.doi.org/10.2214/ajr.147.1.103>.
- Duyn, J.H., van Gelderen, P., Li, T.-Q., de Zwart, J.A., Koretsky, A.P., Fukunaga, M., 2007. High-field MRI of brain cortical substructure based on signal phase. *Proc. Natl. Acad. Sci. U. S. A.* 104, 11796–11801. <http://dx.doi.org/10.1073/pnas.0610821104>.
- Gelman, N., Gorell, J.M., Barker, P.B., Savage, R.M., Spickler, E.M., Windham, J.P., Knight, R.A., 1999. MR imaging of human brain at 3.0 T: preliminary report on transverse relaxation rates and relation to estimated iron content. *Radiology* 210, 759–767. <http://dx.doi.org/10.1148/radiology.210.3.r99fe41759>.
- Haacke, E.M., Xu, Y., Cheng, Y.-C.N., Reichenbach, J.R., 2004. Susceptibility weighted imaging (SWI). *Magn. Reson. Med.* 52, 612–618. <http://dx.doi.org/10.1002/mrm.20198>.
- Haacke, E.M., Cheng, N.Y.C., House, M.J., Liu, Q., Neelavalli, J., Ogg, R.J., Khan, A., Ayaz, M., Kirsch, W., Obenaus, A., 2005. Imaging iron stores in the brain using magnetic resonance imaging. *Magn. Reson. Imaging* 23, 1–25. <http://dx.doi.org/10.1016/j.mri.2004.10.001>.
- Haacke, E.M., Ayaz, M., Khan, A., Manova, E.S., Krishnamurthy, B., Gollapalli, L., Ciulla, C., Kim, I., Petersen, F., Kirsch, W., 2007. Establishing a baseline phase behavior in magnetic resonance imaging to determine normal vs. abnormal iron content in the brain. *J. Magn. Reson. Imaging* 26, 256–264. <http://dx.doi.org/10.1002/jmri.20987>.
- Hallgren, B., Sourander, P., 1958. The effect of age on the non-haem iron in the human brain. *J. Neurochem.* 3, 41–51.
- Jenkinson, M., 2003. Fast, automated, N-dimensional phase-unwrapping algorithm. *Magn. Reson. Med.* 49, 193–197. <http://dx.doi.org/10.1002/mrm.10354>.
- Khalil, M., Langkammer, C., Ropele, S., Petrovic, K., Wallner-Blazek, M., Löffelner, M., Jehna, M., Bachmaier, G., Schmidt, R., Enzinger, C., Fuchs, S., Fazekas, F., 2011. Determinants of brain iron in multiple sclerosis: a quantitative 3 T MRI study. *Neurology* 77, 1691–1697. <http://dx.doi.org/10.1212/WNL.0b013e318236e0fe>.
- Kressler, B., de Rochefort, L., Liu, T., Spincemaille, P., Jiang, Q., Wang, Y., 2010. Nonlinear regularization for per voxel estimation of magnetic susceptibility distributions from MRI field maps. *IEEE Trans. Med. Imaging* 29, 273–281. <http://dx.doi.org/10.1109/TMI.2009.2023787>.
- Langkammer, C., Krebs, N., Goessler, W., Scheurer, E., Ebner, F., Yen, K., Fazekas, F., Ropele, S., 2010. Quantitative MR imaging of brain iron: a postmortem validation study. *Radiology* 257, 455–462. <http://dx.doi.org/10.1148/radiol.10100495>.
- Langkammer, C., Schweser, F., Krebs, N., Deistung, A., Goessler, W., Scheurer, E., Sommer, K., Reishofer, G., Yen, K., Fazekas, F., Ropele, S., Reichenbach, J.R., 2012. Quantitative susceptibility mapping (QSM) as a means to measure brain iron? A post mortem validation study. *Neuroimage* 62, 1593–1599. <http://dx.doi.org/10.1016/j.neuroimage.2012.05.049>.
- Lebel, R.M., Eissa, A., Seres, P., Blevins, G., Wilman, A.H., 2012. Quantitative high-field imaging of sub-cortical gray matter in multiple sclerosis. *Mult. Scler.* 18, 433–441. <http://dx.doi.org/10.1177/1352458511428464>.
- LeVine, S.M., 1997. Iron deposits in multiple sclerosis and Alzheimer's disease brains. *Brain Res.* 760, 298–303. [http://dx.doi.org/10.1016/S0006-8993\(97\)00470-8](http://dx.doi.org/10.1016/S0006-8993(97)00470-8).
- Li, L., Leigh, J.S., 2004. Quantifying arbitrary magnetic susceptibility distributions with MR. *Magn. Reson. Med.* 51, 1077–1082. <http://dx.doi.org/10.1002/mrm.20054>.
- Li, T.Q., Yao, B., van Gelderen, P., Merkle, H., Dodd, S., Talagala, L., Koretsky, A.P., Duyn, J., 2009. Characterization of T(2)* heterogeneity in human brain white matter. *Magn. Reson. Med.* 62, 1652–1657. <http://dx.doi.org/10.1002/mrm.22156>.
- Li, W., Wu, B., Liu, C., 2011. Quantitative susceptibility mapping of human brain reflects spatial variation in tissue composition. *Neuroimage* 55, 1645–1656. <http://dx.doi.org/10.1016/j.neuroimage.2010.11.088>.
- Li, W., Wu, B., Batrachenko, A., 2014. Differential developmental trajectories of magnetic susceptibility in human brain gray and white matter over the lifespan. *Hum. Brain Mapp.* 35, 2698–2713. <http://dx.doi.org/10.1002/hbm.22360> (Differential).
- Liu, T., Spincemaille, P., de Rochefort, L., Kressler, B., Wang, Y., 2009. Calculation of susceptibility through multiple orientation sampling (COSMOS): a method for conditioning the inverse problem from measured magnetic field map to susceptibility source image in MRI. *Magn. Reson. Med.* 61, 196–204. <http://dx.doi.org/10.1002/mrm.21828>.
- Liu, T., Liu, J., de Rochefort, L., Spincemaille, P., Khalidov, I., Ledoux, J.R., Wang, Y., 2011. Morphology enabled dipole inversion (MED) from a single-angle acquisition: comparison with COSMOS in human brain imaging. *Magn. Reson. Med.* 66, 777–783. <http://dx.doi.org/10.1002/mrm.22816>.
- Marques, J.P., Maddage, R., Mlynarik, V., Gruetter, R., 2009. On the origin of the MR image phase contrast: an *in vivo* MR microscopy study of the rat brain at 14.1 T. *Neuroimage* 46, 345–352. <http://dx.doi.org/10.1016/j.neuroimage.2009.02.023>.

- Meguro, R., Asano, Y., Odagiri, S., Li, C., Iwatsuki, H., Shoumura, K., 2007. Nonheme-iron histochemistry for light and electron microscopy: a historical, theoretical and technical review. *Arch. Histol. Cytol.* 70, 1–19. <http://dx.doi.org/10.1679/aohc.70.1>.
- Mitsumori, F., Watanabe, H., Takaya, N., Garwood, M., Auerbach, E.J., Michaeli, S., Mangia, S., 2012. Toward understanding transverse relaxation in human brain through its field dependence. *Magn. Reson. Med.* 68, 947–953. <http://dx.doi.org/10.1002/mrm.23301>.
- Ogg, R.J., Langston, J.W., Haacke, E.M., Steen, R.G., Taylor, J.S., 1999. The correlation between phase shifts in gradient-echo MR images and regional brain iron concentration. *Magn. Reson. Imaging* 17, 1141–1148. [http://dx.doi.org/10.1016/S0730-725X\(99\)00017-X](http://dx.doi.org/10.1016/S0730-725X(99)00017-X).
- Peran, P., Hagberg, G., Luccichenti, G., Cherubini, A., Brainovich, V., Celsis, P., Caltagirone, C., Sabatini, U., 2007. Voxel-based analysis of R²* maps in the healthy human brain. *J. Magn. Reson. Imaging* 26, 1413–1420. <http://dx.doi.org/10.1002/jmri.21204>.
- Rauscher, A., Sedlacik, J., Barth, M., Mentzel, H.-J., Reichenbach, J.R., 2005. Magnetic susceptibility-weighted MR phase imaging of the human brain. *AJNR Am. J. Neuroradiol.* 26, 736–742 (doi:26/4/736 [pii]).
- Reichenbach, J.R., 2012. The future of susceptibility contrast for assessment of anatomy and function. *Neuroimage* 62, 1311–1315. <http://dx.doi.org/10.1016/j.neuroimage.2012.01.004>.
- Robinson, S., Grabner, G., Witoszynskyj, S., Trattnig, S., 2011. Combining phase images from multi-channel RF coils using 3D phase offset maps derived from a dual-echo scan. *Magn. Reson. Med.* 65, 1638–1648. <http://dx.doi.org/10.1002/mrm.22753>.
- Schenck, J.F., Zimmerman, E.A., 2004. High-field magnetic resonance imaging of brain iron: birth of a biomarker? *NMR Biomed.* 17, 433–445. <http://dx.doi.org/10.1002/nbm.922>.
- Schweser, F., Deistung, A., Lehr, B.W., Reichenbach, J.R., 2011. Quantitative imaging of intrinsic magnetic tissue properties using MRI signal phase: an approach to in vivo brain iron metabolism? *Neuroimage* 54, 2789–2807. <http://dx.doi.org/10.1016/j.neuroimage.2010.10.070>.
- Shmueli, K., de Zwart, J.A., van Gelderen, P., Li, T.-Q., Dodd, S.J., Duyn, J.H., 2009. Magnetic susceptibility mapping of brain tissue in vivo using MRI phase data. *Magn. Reson. Med.* 62, 1510–1522. <http://dx.doi.org/10.1002/mrm.22135>.
- Smith, S.M., 2002. Fast robust automated brain extraction. *Hum. Brain Mapp.* 17, 143–155. <http://dx.doi.org/10.1002/hbm.10062>.
- Stephenson, E., Nathoo, N., Mahjoub, Y., Dunn, J.F., Yong, V.W., 2014. Iron in multiple sclerosis: roles in neurodegeneration and repair. *Nat. Rev. Neurol.* <http://dx.doi.org/10.1038/nrneurol.2014.118>.
- Sun, H., Wilman, A.H., 2013. Background field removal using spherical mean value filtering and Tikhonov regularization. *Magn. Reson. Med.* 1157, 1151–1157. <http://dx.doi.org/10.1002/mrm.24765>.
- Thomas, L.O., Boyko, O.B., Anthony, D.C., Burger, P.C., 1993. MR detection of brain iron. *AJNR Am. J. Neuroradiol.* 14, 1043–1048.
- Van Duijn, S., Nabuurs, R.J.A., van Rooden, S., Maat-Schieman, M.L.C., van Duinen, S.G., van Buchem, M.A., van der Weerd, L., Natté, R., 2011. MRI artifacts in human brain tissue after prolonged formalin storage. *Magn. Reson. Med.* 65, 1750–1758. <http://dx.doi.org/10.1002/mrm.22758>.
- Walsh, A.J., Lebel, R.M., Eissa, A., Blevins, G., Catz, I., Lu, J.-Q., Resch, L., Johnson, E.S., Emery, D.J., Warren, K.G., Wilman, A.H., 2013. Multiple sclerosis: validation of MR imaging for quantification and detection of iron. *Radiology* 267, 531–542. <http://dx.doi.org/10.1148/radiol.12120863>.
- Wharton, S., Bowtell, R., 2010. Whole-brain susceptibility mapping at high field: a comparison of multiple- and single-orientation methods. *Neuroimage* 53, 515–525. <http://dx.doi.org/10.1016/j.neuroimage.2010.06.070>.
- Williams, R., Buchheit, C.L., Berman, N.E.J., LeVine, S.M., 2012. Pathogenic implications of iron accumulation in multiple sclerosis. *J. Neurochem.* 120, 7–25. <http://dx.doi.org/10.1111/j.1471-4159.2011.07536.x>.
- Wu, B., Li, W., Guidon, A., Liu, C., 2012. Whole brain susceptibility mapping using compressed sensing. *Magn. Reson. Med.* 67, 137–147. <http://dx.doi.org/10.1002/mrm.23000>.
- Yao, B., Li, T., Gelderen, P. Van, Shmueli, K., de Zwart, J.A., Duyn, J.H., 2009. Susceptibility contrast in high field MRI of human brain as a function of tissue iron content. *Neuroimage* 44, 1259–1266. <http://dx.doi.org/10.1016/j.neuroimage.2008.10.029>.
- Zhang, Y., Zabad, R.K., Wei, X., Metz, L.M., Hill, M.D., Mitchell, J.R., 2007. Deep grey matter “black T2” on 3 tesla magnetic resonance imaging correlates with disability in multiple sclerosis. *Mult. Scler. (Houndmills, Basingstoke, England)* <http://dx.doi.org/10.1177/1352458507076411>.
- Zheng, W., Nichol, H., Liu, S., Cheng, Y.-C.N., Haacke, E.M., 2013. Measuring iron in the brain using quantitative susceptibility mapping and X-ray fluorescence imaging. *Neuroimage* 78, 68–74. <http://dx.doi.org/10.1016/j.neuroimage.2013.04.022>.